Spin currents in Pt/Co/Pt trilayers

H.C. Overweg

July 5, 2011

Magnetic and Superconducting Materials group
This project was supervised by:
MSc. T.G.A. Verhagen
Prof. Dr. J. Aarts

Contents

1 Introduction

1.1 Giant Magnetoresistance

One of the biggest discoveries in spintronics in the last century is the giant Magnetoresistance, discovered at the end of the eighties by Baibich *et al.* [1] and Binasch *et al.* [2]. It is a magnetoresistance effect observed in thin films, composed of alternating ferromagnetic and nonmagnetic layers. External magnetic fields can manipulate the orientation of the ferromagnetic layers. The resistance of the structure shown in Figure 1a is low when the spins of the ferromagnetic layers are aligned parallel and high when the spins are aligned anti-parallel. Figure 1b shows the difference in resistance of the two configurations as a function of the magnetic field strength. By fixing the spins in one of the ferromagnets and allowing the spins in the second layer to rotate, the magnetization direction of the second ferromagnet can be measured by a change in the resistance. Read heads of hard disks exploit this effect to measure the relative orientation of the magnetic grains on a hard disk that represent bits [3].

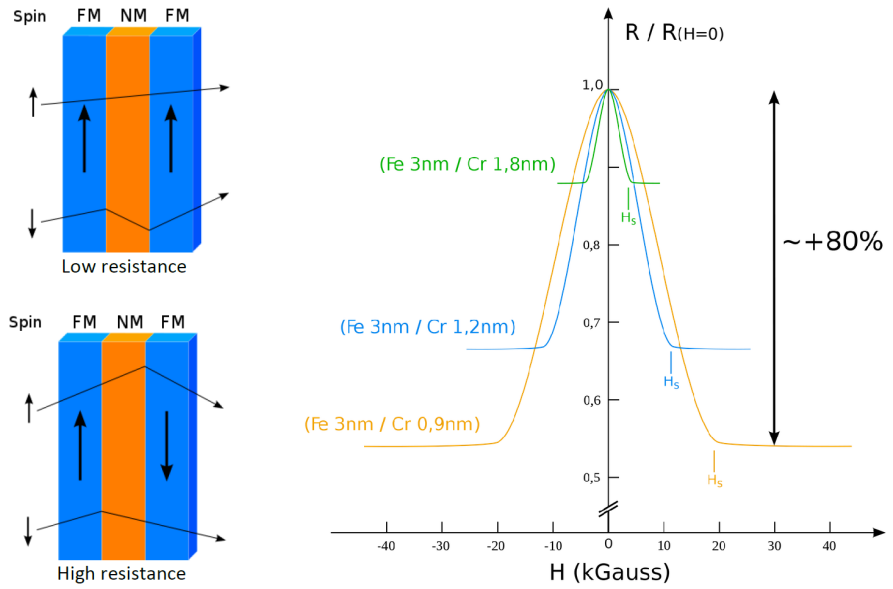

Figure 1: Giant Magnetoresistance. (a) When the spins of the two ferromagnetic layers are aligned parallel (upper figure), the resistance is lower than in the anti-parallel case (lower figure). (b) The resistance R as a function of the applied magnetic field H, when the zero-field state is anti-parallel.

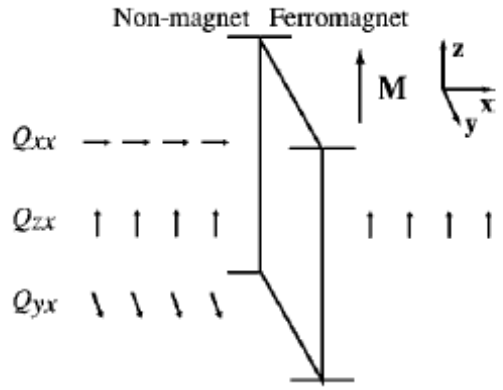

Figure 2: Three states of spin current scatter from an interface. The currents flow from left to right, from the normal metal into the ferromagnet. Q_{zx} is longitudinal (parallel) to the magnetization $\boldsymbol{M}$. Q_{xx} Q_{yx} are transverse to $\boldsymbol{M}$. Only Q_{zx} can be nonzero in the bulk of the magnet. The transverse spin currents are absorbed in the interfacial region. Figure from [4].

1.2 Current induced switching

In the nineties it was discovered that electric currents can reorient ferromagnetic order in multilayer structures. Tsoi et al. [5] demonstrated magnetization precession in $(\mathrm{Co/Cu})_n$ multilayers with a current injected with a point contact [6].
When a spin-polarised current flows from a normal metal into a ferromagnet, it exerts a torque on the magnetization of the ferromagnet. This torque is called the spin transfer torque. The torque is caused by the transfer of spin angular momentum from the conduction electrons to the magnetization of the ferromagnet. When a spin-polarised current is injected into a ferromagnet, only the component parallel to the magnetization of the ferromagnet is transmitted, as is shown in Figure 2. The magnet absorbs the transverse components of the spin in the region near the interface. This causes a torque on the magnetization.

Spin pumping and the inverse spin Hall effect

Spin pumping is the inverse process of a spin transfer torque. Whereas a spin current exerts a torque on a ferromagnet, a precessing magnetization $\boldsymbol{M}(t)$ loses torque by emitting a spin current $\boldsymbol{J}_s$ into the adjacent layers (see Figure 3a). As can be seen in this figure, electrons with opposite spins are travelling in opposite directions in the normal metal layers. Therefore, the spin-orbit coupling deflects the electrons in the same direction and a charge current $\boldsymbol{J}_c$ perpendicular to the spin current is induced (see Figure 3b). This is called the inverse spin Hall effect (ISHE).

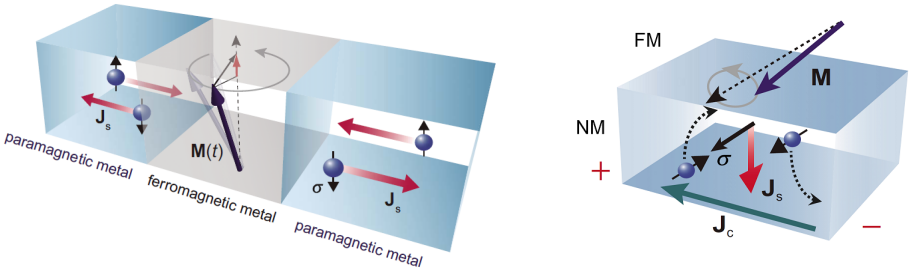

(a) **(b)**

Figure 3: (a) A precessing magnetization emits a spincurrent $\boldsymbol{J}_s$ into the adjacent layers. (b) Due to spin-orbit coupling, the spins are deflected in the same direction. This causes a charge current $\boldsymbol{J}_c$ perpendicular to the spin current $\boldsymbol{J}_s$[7].

1.3 Outline of this project

The spin current in a multilayer depends on several factors, such as the amount of precession, the ability of the nonmagnetic layers to absorb the current and the quality of the interface. In this Bachelor project the main question is what the dependence is of the spin current on the thickness of the ferromagnetic layer. Furthermore we tried to measure the voltage induced by the inverse spin Hall effect by applying contacts to the normal metal layer.

2 Theory

2.1 Magnets

Three principal sources are responsible for the magnetic moment of a free atom: the spin of the electrons; their orbital angular momentum and the change in orbital moment as a consequence of an applied magnetic field. The magnetization $\boldsymbol{M}$ in a solid is the magnetic moment per unit volume. The magnetic susceptibility χ per unit volume is defined as:

$$\chi = \frac{M}{H_a} \tag{1}$$

where H_a is the applied magnetic field. Substances with a negative susceptibility are called diamagnets, substances with a positive susceptibility are called paramagnets.
A third type of magnetism is ferromagnetism. Ferromagnets exhibit magnetic moment even if zero magnetic field is applied when the temperature T is below their Curie temperature T_c. At higher temperatures ferromagnets become paramagnetic [8].

2.2 Ferromagnetic resonance

When a static magnetic field is applied to a ferromagnet, the magnetization precesses around the direction of the static field. Furthermore, an energy difference between the two spin states is created due to Zeeman splitting. The energy difference ΔE between these two levels is proportional to the magnetic field strength B: $\Delta E = \hbar\gamma B$ where γ is the gyromagnetic ratio. Microwave radiation of angular frequency ω that fulfils the resonance condition $\omega = \gamma B$ can be absorbed by the sample and can cause the spins to flip. When working at constant frequency, sweeping the field will lead to absorption of microwave radiation at the field strength which matches the energy gap. This is shown in Figure 4.

In thermal equilibrium, the magnetization $\boldsymbol{M}$ obeys the Landau-Lifshitz equation:

$$\frac{d\boldsymbol{m}}{dt} = -\gamma \boldsymbol{m} \times \boldsymbol{B} \tag{2}$$

in which $\boldsymbol{m} = \boldsymbol{M}/|\boldsymbol{M}|$ is the direction of the magnetization, γ the gyromagnetic ratio and $\boldsymbol{B}$ the effective magnetic field, composed of the external magnetic field, the demagnetising field induced by $\boldsymbol{M}$ and the crystal anisotropy field [9].

Because the itinerant electrons do not adjust instantaneously to the varying magnetization, an additional damping term is needed [6]. This additional term can be described by a torque of the form:

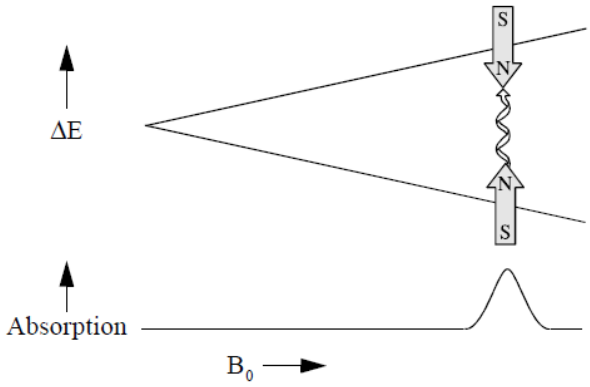

Figure 4: Absorption of radiation occurs in a ferromagnet at the magnetic field strength where the resonance condition $\omega = \gamma B$ is fulfilled.

$$\alpha \boldsymbol{m} \times \frac{d\boldsymbol{m}}{dt} \tag{3}$$

where α is the Gilbert damping constant.

Together, equation 2 and equation 3 form the Landau-Lifshitz-Gilbert equation:

$$\frac{d\boldsymbol{m}}{dt} = -\gamma \boldsymbol{m} \times \boldsymbol{B} + \alpha \boldsymbol{m} \times \frac{d\boldsymbol{m}}{dt} \tag{4}$$

2.3 Damping

A measurement of the spectrum of the absorbed radiation is a measure for the Gilbert damping constant. In analogy to a harmonic oscillator, a larger damping constant α leads to a shorter oscillation in the time domain, which yields a broader peak in the frequency domain.
Several factors affect the damping constant α.

- In the first place, a ferromagnet shows intrinsic Gilbert damping. Usually, the value for α is extracted from the FMR peak width ΔB using the relation:

  $$\Delta B = \frac{\alpha}{\gamma}\omega \tag{5}$$

  with ω the angular frequency of the microwave radiation. The intrinsic damping constant is material dependent. The bulk value for Co is $\alpha \approx 5 \cdot 10^{-4}$ [9].

- A magnetic field that changes in time induces a current in a conducting material, a so called eddy current. In ferromagnetic layers of $d > 50$ nm the damping constant increases, due to eddy currents in the film

[10]. The damping constant of the eddy current α_{ed} is proportional to the square of the thickness of the ferromagnetic layer d $\alpha_{ed} \sim d^2$ [11].

- As described in the introduction, the magnetization can lose torque by emitting a spin current. Therefore, a spin current increases the damping. This damping constant $\alpha_{\boldsymbol{J}_s}$ is proportional to the inverse of the thickness $\alpha_{\boldsymbol{J}_s} \sim d^{-1}$ [9]. The amount of spin current itself depends on several factors, which are described in the next section.

- When a spin current is emitted from a ferromagnetic layer into a normal metal, it creates some spin accumulation in the normal metal. This accumulation induces a backflow spin current $\boldsymbol{J}_s^{back}$ (see Figure 5) [12]. The current flows back into the ferromagnet and exert a torque on the magnetization (a spin transfer torque). This also affects the damping constant. When the normal metal can flip the absorbed spins from the ferromagnet relatively easy, this contribution is negligibly small.

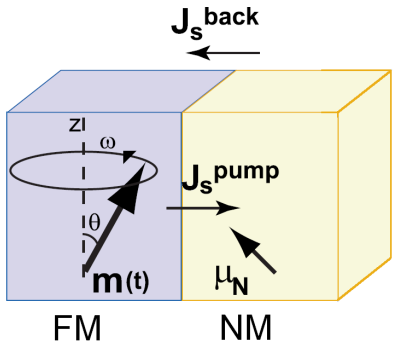

Figure 5: The precession of the magnetization in the FM layer pumps spin current $\boldsymbol{J}_s$ into the NM layer, thereby creating spin accumulation μ_N in the NM layer. This accumulation induces a backward spin current $\boldsymbol{J}_s^{back}$. Figure from [12].

In summary, the behaviour of the damping constant as a function of the F-layer thickness should theoretically take the form of Figure 6.For a thin F-layer, the influence of the spin pumping dominates, which causes extra damping and hence a broader peak. The intrinsic value for a F-layer without a normal metal to absorb spin currents is much lower. As the layer thickness increases, the influence of the spin current decreases. At a layer thickness of more than 50 nm, the effect of the eddy currents becomes significant and increases the damping constant again.

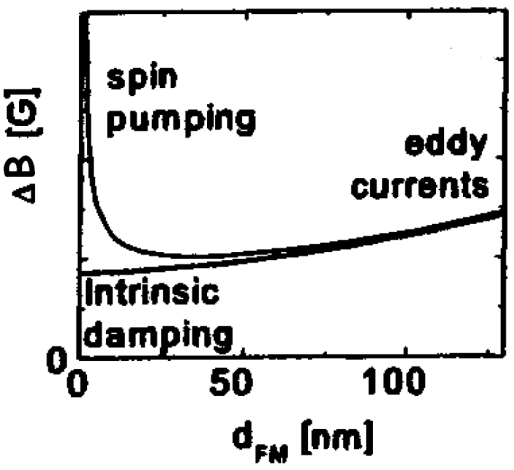

Figure 6: FMR peak width ΔB of a F/N bilayer as a function of the thickness d of the ferromagnetic layer. Three regimes are distinguishable. For thin films $d \approx \min\{\lambda_{sf}, \lambda_J\}$, the damping caused by spin current dominates. For $d \gg \min\{\lambda_{sf}, \lambda_J\}$, intrinsic damping is visible and for $d > 50nm$ we see the influence of eddy currents [10].

2.4 Spin pumping

When the magnetization of a ferromagnet is precessing, it loses torque by emitting a spin current into the adjacent normal metal layer (see Figure 7).

It is therefore not surprising that a spin current $\boldsymbol{J}_s$ at the interface between a normal metal and a ferromagnet is proportional to the loss of magnetization:

$$\boldsymbol{J}_s \sim \boldsymbol{m} \times \frac{d\boldsymbol{m}}{dt} \tag{6}$$

The spin current adds up to the damping term of the Landau-Lifshitz-Gilbert equation (equation 3) and consequently enhances α.
A factor that plays an important role in the amount of spin current that is created, is the capability of the normal metal to absorb a spin current. When using a metal with a fast spin-flip relaxation time, the injection of spin into this metal can be balanced by relaxation of the spins. Such metals are called good spin sinks. Pt and Pd are examples of good spin sinks, since they have strong spin-orbit coupling. On the other hand, metals such as Al and Cu absorb spin currents to a much smaller extent, because they have much weaker spin-orbit coupling. When a spin current is injected in a bad spin sink, accumulation of the spin occurs, and no more spin current can flow into the normal metal. In the case of a bad spin sink, no or little enhancement of the damping constant will occur [3].

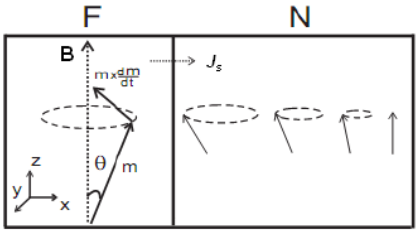

Figure 7: The precession of the magnetization $\boldsymbol{M}$ in the ferromagnet F pumps a spin current $\boldsymbol{J}_s$ into the normal metal N. In the normal metal the spins relax to their equilibrium position[3].

As Figure 2 shows, in the case of injection of a spin current only transverse components create a torque. In the spin pumping case, the torque only creates transverse spin accumulation, i.e. perpendicular to the net magnetic moment. Longitudinal spin accumulation decays at the length scale of the spin diffusion length λ_{sd}, which is about 60 nm for Co. However, the transverse accumulation decays much faster, at a scale of the minimum of the spin flip length λ_{sf} and the spin coherence length λ_J [13]. The spin coherence length of Co is approximately 2 nm, thus spin currents only play a role in the region very close to the interface. When using a much thicker Co layer, $d \gg \min\{\lambda_{sf}, \lambda_J\}$ the total magnetization is less sensitive to a loss of torque in the region near the interface [9]. Even though a spin current flows in the region near the interface, a much larger part of the ferromagnet does not experience the effect of the spin current, the extra damping. So with increasing thickness of the Co layer, we expect a smaller contribution to the damping constant of the spin pumping.

2.5 Inverse spin Hall effect

In a spin current, electrons with opposite spins travel in opposite directions. Therefore, their spin-orbit coupling deflects the electrons in the same directions (see Figure 8). A charge current $\boldsymbol{J}_c$ is induced in the normal metal, which is proportional to:

$$\boldsymbol{J}_c \sim \boldsymbol{J}_s \times \boldsymbol{\sigma} \tag{7}$$

where $\boldsymbol{\sigma}$ is the spin-current polarisation. When changing the direction of the external magnetic field by 180°, the direction of the spin current polarisation is changed. Since the sign of the spin current $\boldsymbol{J}_s$ is unaltered, the charge current $\boldsymbol{J}_c$ changes sign. Therefore, the measured voltage shows a

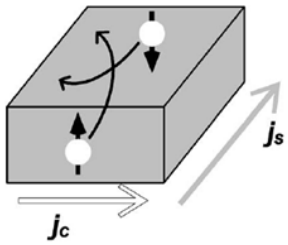

Figure 8: Inverse spin Hall effect on two electrons with opposite spin. A charge current $\boldsymbol{j}_c$ is induced perpendicular to the spin current $\boldsymbol{j}_s$. Figure from [14].

sign change when turning the direction of the magnetic field relative to the sample.

2.6 Anomalous Hall effect

The electric field of the microwave radiation generates a current in the ferromagnet. The electrons are scattered by the spin-orbit interaction at impurities. This induces a voltage in the same direction as the inverse spin Hall voltage. This effect is called the anomalous Hall effect. Whereas the voltage of the inverse spin Hall effect is symmetric when going through resonance, the anomalous Hall effect shows an asymmetric voltage (see Figure 9). This is explained by the fact that the phase difference between the microwave radiation and the magnetization-precession changes by π at resonance [14].

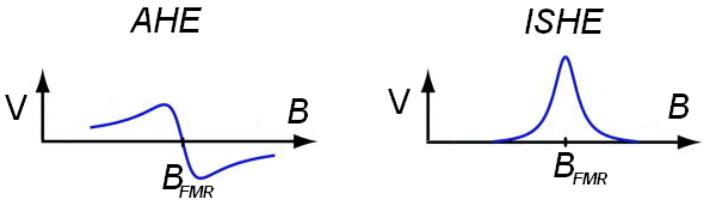

Figure 9: It is easy to distinguish between the contribution of the voltage of the anomalous Hall effect and the inverse spin Hall effect, since the voltage induced by anomalous Hall effect is antisymmetric around the resonance field and the voltage of the inverse spin Hall effect is symmetric.

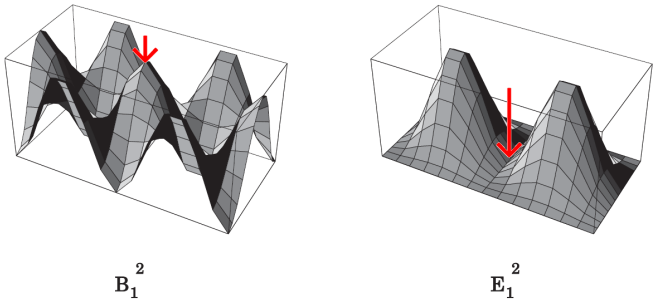

Figure 10: Magnetic and electric field distribution in the cavity. The red arrow marks the position of the sample.

3 Experimental

3.1 Samples

The fabricated samples consisted of F/N metal bilayers and N/F/N trilayers. Co is used as the ferromagnet and the normal metals are Pt and Cu . The substrates were cut from a silicon wafer with a native oxide layer into pieces of 2×2 mm^2 with a diamond pencil. They were cleaned by ultrasonic cleaning with acetone and isopropanol. Thin films were deposited on the silicon substrates via RF diode sputtering with Ar in a Leybold Z-400 at a base pressure of approximately 8×10^{-6} mbar. An overview of the samples used in the experiments can be found in Appendix A. The thickness of the layers of some samples are verified with x-ray reflectometry.

3.2 Ferromagnetic resonance measurement

The ferromagnetic resonance experiments were performed in a magnetic resonance spectrometer (Bruker EMX) in the X-band frequency range (~ 9 GHz) with a water cooled magnet (Bruker ER 070). All measurements were performed at room temperature. The sample is placed in a TE_{102} microwave cavity. The distribution of the electric and magnetic field of the microwave radiation is shown in Figure 10. We tried to locate the sample at the centre of the cavity, so that it is located in a antinode of the microwave magnetic field and an node of the microwave electric field. This should reduce the influence of the anomalous Hall effect.

The FMR measurements were recorded using frequency modulation and phase sensitive lock-in detection. The modulation frequency of the microwave radiation was 100 kHz and the modulation amplitude was in the range of 0.1-1.0 mT during all measurements. A scheme of the set-up is shown in

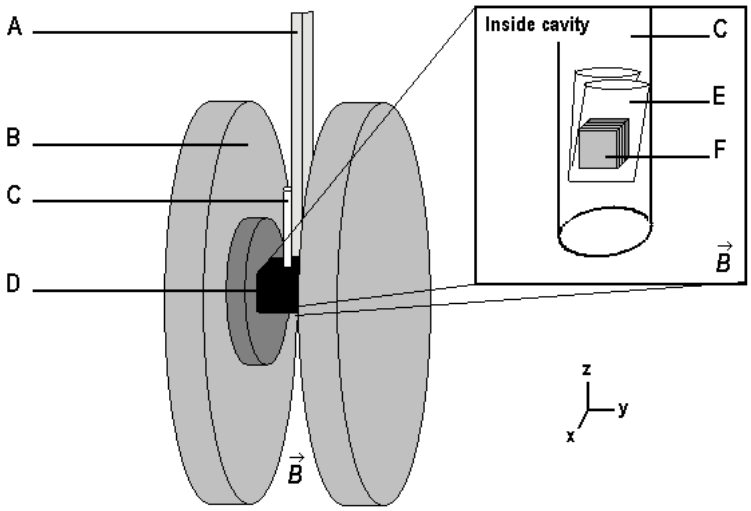

Figure 11: Schematic overview of the set-up. A) is the waveguide that transports the microwave radiation. The radiation enters the cavity at the back-side. B) is the magnet, creating a magnetic field in the y-direction. C) is the quartz tube containing the sample. D) is the cavity. E) is the drinking straw that holds the sample F).

Figure 11. The samples were placed in a quartz tube with an outer diameter of 10 mm, using a part of a transparent drinking straw to keep them in place.

3.3 Voltage measurement

To measure the inverse spin Hall voltage V, the sample is glued with varnish (GE/IMI 7031) on a quartz rod with a quartz tube attached to it. Twisted Cu wires are attached to both ends of the sample with silver paint.Figure 12a shows a sketch of the sample with contacts. The samples are covered with teflon tape. A picture of the sample with contacts is shown in Figure 12b.
The FMR measurements are performed, while simultaneously the voltage V over the sample is measured with a Keithley 2182 nanovoltmeter. To synchronise these measurements, we used a Labview program to trigger the magnetic resonance spectrometer externally.

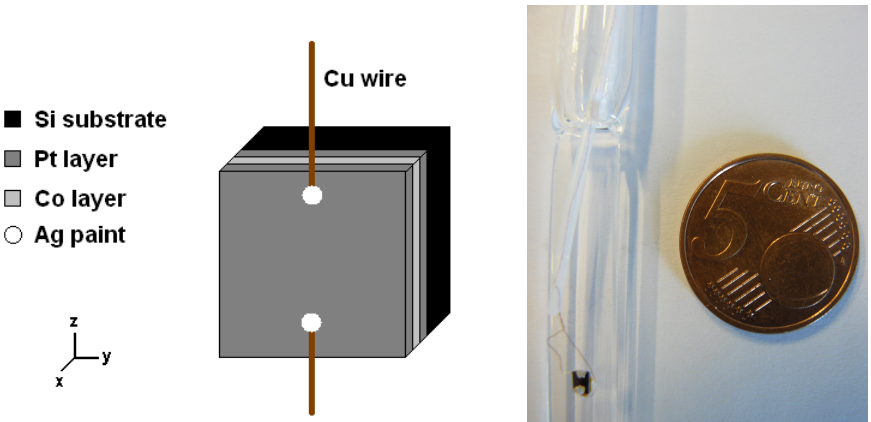

(a) **(b)**

Figure 12: Sample holder and sample with Cu wires attached to it.

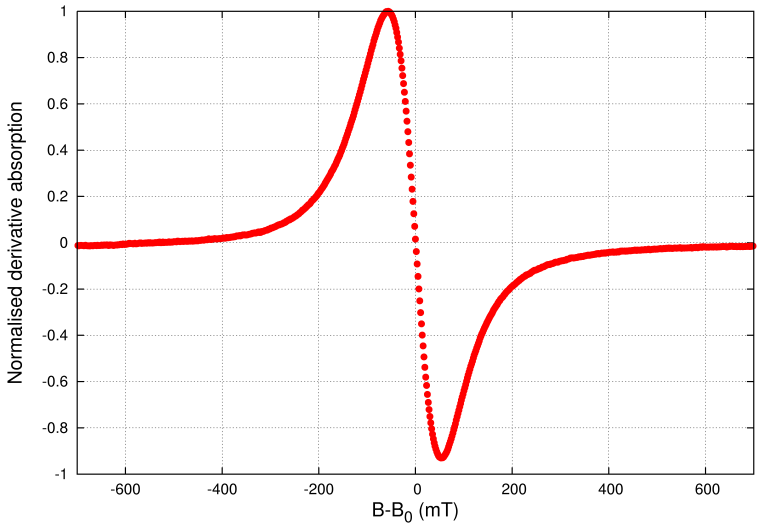

Figure 13: A first derivative spectrum of the absorbed microwave radiation as a function of the applied magnetic field for a sample Pt(10)/Co(6)/Pt(10) of batch N. The value of B_0 was 72 mT.

4 Results

4.1 Normalisation procedure

To simplify the comparison of different spectra, the following normalisation procedure is used: The data point closest to the x-axis was determined, and this point was shifted to the origin by subtracting its x-value B_0, which is usually $B_0 \approx 60$ mT. In the y-direction, the peaks are normalised by dividing each value by the maximum value.

4.2 FMR parameters

Figure 13 shows a typical absorption curve of the microwave radiation. It is a first-derivative spectrum: it shows the first derivative of the intensity of the absorbed radiation as a function of the external magnetic field. A sample of batch N is used (see appendix A).

The peak width (or rather peak-to-dip width) was found to be $\Delta B = 10.9$ mT.

In Figure 14, the FMR spectrum as a function of the angle between the sample plane and the magnetic field direction is plotted. It was measured with a Co(12)/Pt(10) sample from batch A. As can be seen, the FMR signal

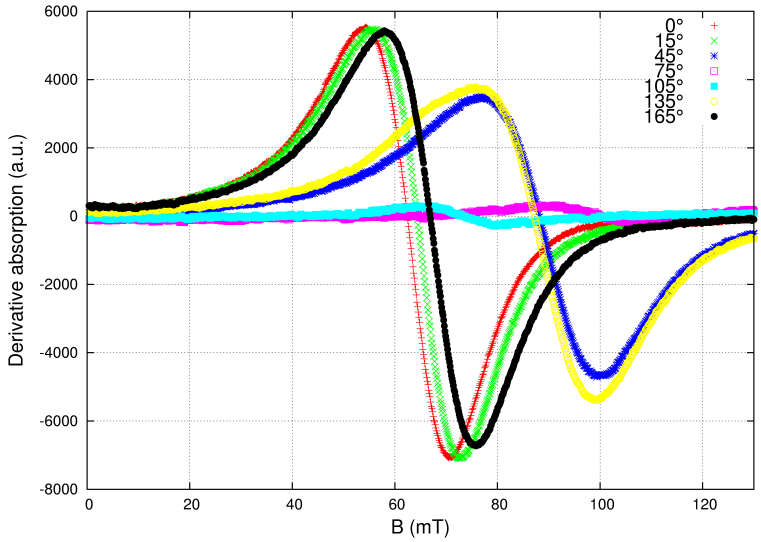

Figure 14: The dependence of the FMR spectrum on the angle between the sample plane and the magnetic field direction for a Co(12)/Pt(10) sample of batch A.

strongly depends on this angle. The center of the absorption peak is at a different field strength for a magnetic field perpendicular or parallel to the sample, just as described by theory [8]. The intensity and the peak width depend on the angle too.

The FMR signal depends only slightly on the heigth of the sample in the cavity in z-direction. This can be seen in Figure 15. This measurement was performed with a Co(70)/Pt(10) sample from batch B. The intersection with the x-axis does not change, which indicates that the resonance frequency does not shift. Moreover, the peak width is unchanged at different heights. Only the intensity of the signal depends on the heigth of the sample, but it is more or less constant over a range of almost a centimeter.

Figure 16 shows that the power of the microwave radiation does not affect the resonance frequency and peak width, as long as saturation does not set in. In the case of this sample, a Pt(10)/Co(12)/Pt(10) sample from batch J, saturation was reached at a microwave power of 80 mW. The intensity of the signal is a linear function of the microwave power in the unsaturated regime. This is shown in Figure 17. When $P > 12$ mW, the peak width broadens due to saturation of the microwave radiation and the peak flattens due to overloading of the lock-in detector.

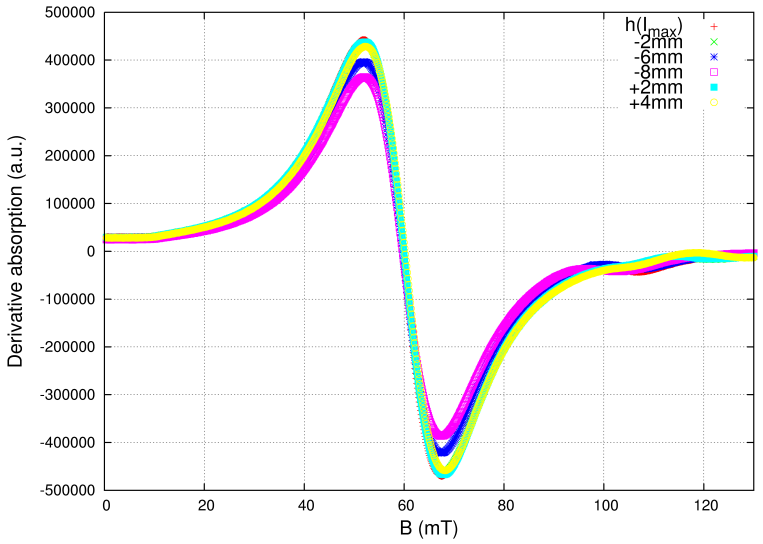

Figure 15: FMR spectrum as a function of the heigth of the sample in the z-direction. A sample of batch B (Co(70)/Pt(10)) was used.

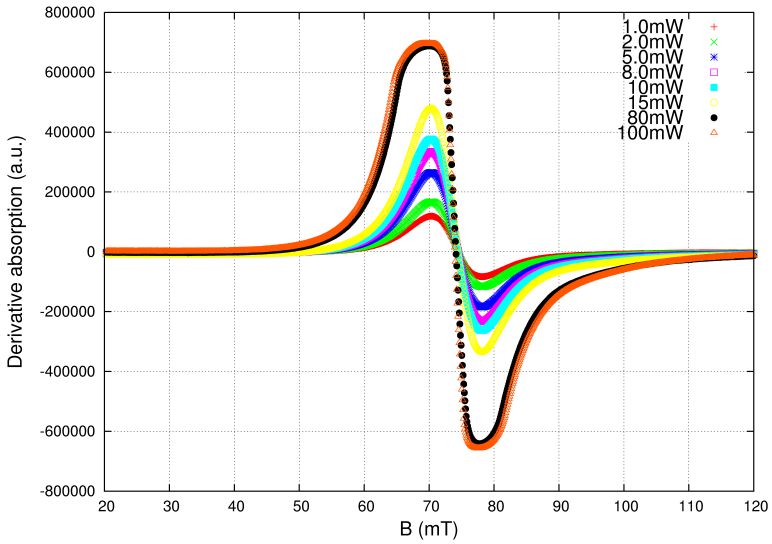

Figure 16: FMR sigal at different intensities of the microwave power measured on a Pt(10)/Co(12)/Pt(10) sample from batch J.

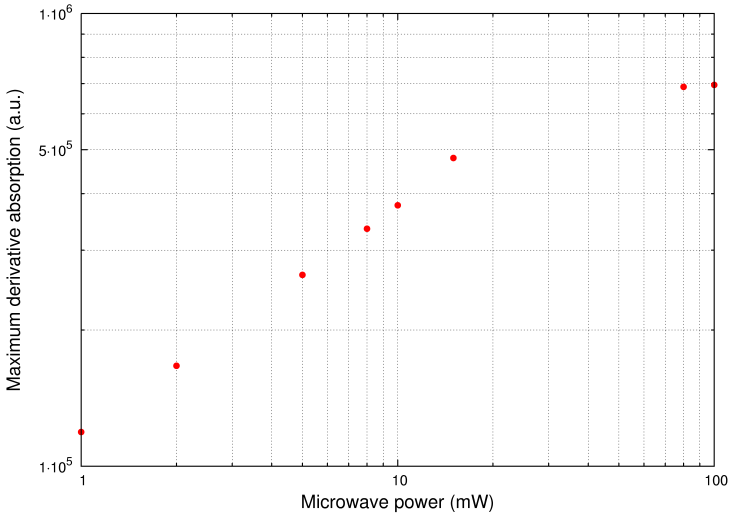

Figure 17: Maximum derivative absorption as a function of the microwave power. In the unsaturated regime, where the microwave power P < 12 mW, the dependence is linear.

Samples with a thick Co layer, sometimes show a second peak in their FMR spectrum. An example is shown in Figure 18, using a Pt(10)/Co(48)/Pt(10) sample from batch R. This peak might be due to other resonant phenomena than ferromagnetic resonance, such as spin waves [15].

In appendix B, FMR spectra of an empty cavity at low and high microwave power, a quartz tube and a quartz tube with Cu wires are shown. The FMR spectrum of the empty cavity at high microwave power indicates that some Cu powder is present in the cavity (causing the peak at 340mT). This does not interfere with our experiments, since we are interested in the region up to 100 mT.

4.3 Thickness dependence of the peak width

In Figure 19 the dependence of the peak width on the thickness of the Co layer in the sample is plotted. The samples consisting of a Pt/Co/Pt trilayer (sample batches A-R, T and U) show the expected behaviour: at small thicknesses, spin pumping plays a significant role, enhancing the damping constant and thus broadening the peak. The peak width falls of quite fast as a function of the thickness and then raises again due to eddy currents, as described on page 8.
The measurement of the Cu/Co/Cu sample (Y) exhibit a smaller peak

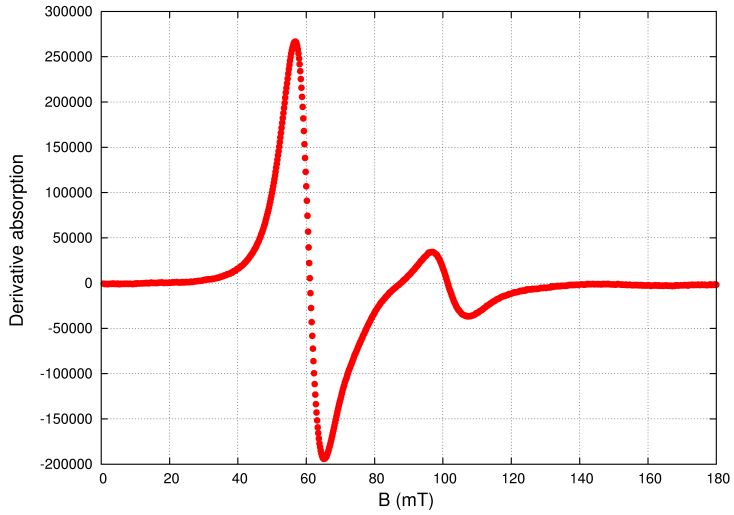

Figure 18: Samples with thick Co layers sometimes show two peaks. The second peak might be due to other resonant phenomena, such as spin waves [15]. The data were taken on a Pt(10)Co(48)Pt(10) sample from batch R.

width, which is explained by the fact that Cu is a poor spin sink and does not absorb spin currents.
Evidently, more spin current is created in the Pt/Co/Cu samples (V) than in the Cu/Co/Pt samples (W), since the former have broader peaks.

As can be seen in Figure 20, the peak width is inversely proportional to the thickness of the F-layer for $d_{Co} < 10$ nm. We have not been able to determine the damping constant α since it depends on a lot of unknown parameters. The relation between the damping constant and the peak width is:

$$\Delta B = \Delta B_0 + \frac{4\pi f}{\sqrt{3}\gamma}\alpha \tag{8}$$

where B_0 is the peak width caused by intrinsic damping, f is the frequency of the microwave radiation and γ is the gyromagnetic ratio[16]. The damping constant is in its turn given by:

$$\alpha = \frac{\gamma}{\gamma_0}\{\alpha_0 + g_L[A_r^{(L)} + A_r^{(R)}]/4\pi M\} \tag{9}$$

where γ is the gyromagnetic ratio, the subscript 0 denotes bulk values, g_L is the Landé factor, A_r are interface parameters, the superscripts (L) and (R) denote parameters evaluated on the left and the right side of the F-layer respectively and M is the total magnetization [9].

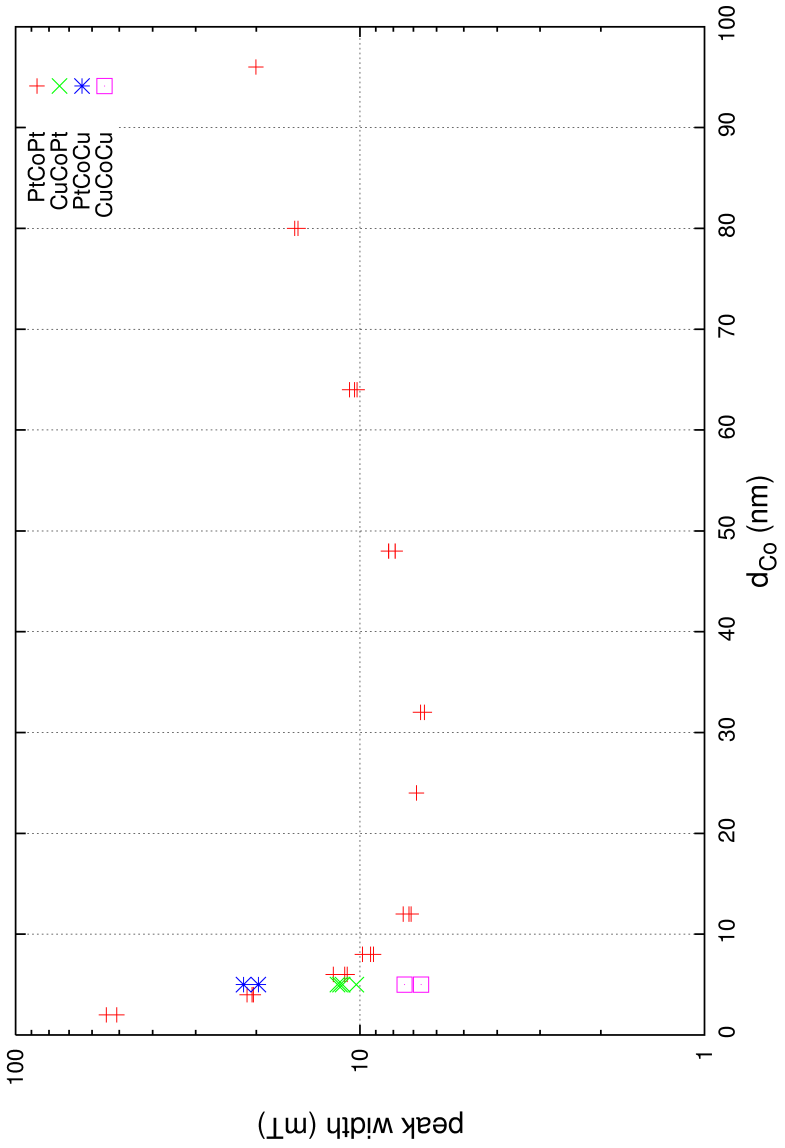

Figure 19: Dependence of the peak-to-peak width on the thickness of the Co layer for samples consisting of Pt/Co/Pt, Pt/Co/Cu, Cu/Co/Pt and Cu/Co/Cu layers. For each thickness and sample type, at least two different samples were measured.

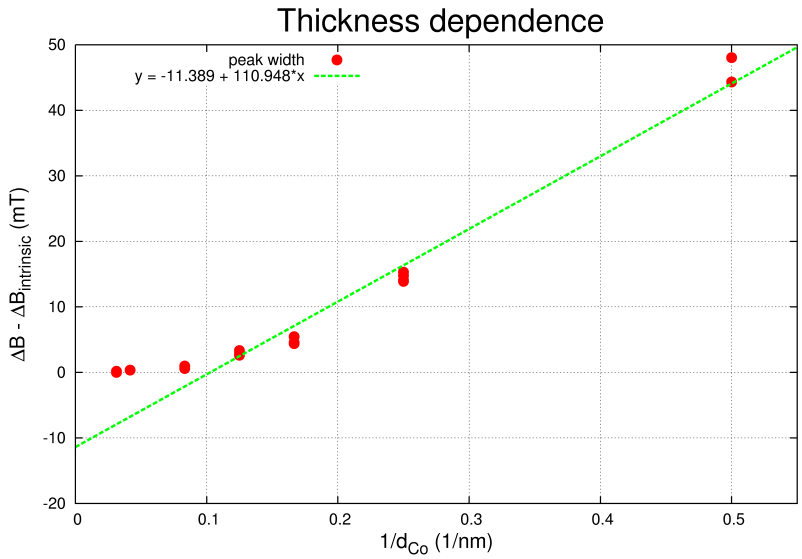

Figure 20: Enhanced peak width as a function of 1/d. The peak width is inversely proportional to the thickness of the F-layer for $d_{Co} < 10$ nm. The fitted function is y = -11.389 + 110.948x.

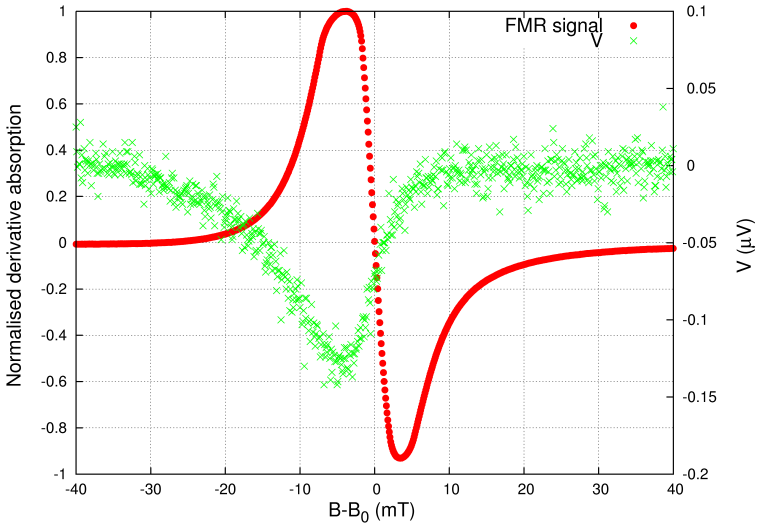

Figure 21: The voltage over the sample (crosses, right hand scale) and the normalized derivative of the absorption (closed circles, left-hand scale) versus the applied field B. The applied field is shifted over a value $B_0 = 70$ mT. The data were taken on a Cu(10)/Co(12)/Pt(10) sample of batch a.

4.4 Measurement of the inverse spin Hall effect

A measurement of the voltage V over the sample (Cu(10)/Co(12)/Pt(10), batch a) is shown in Figure 21. It should be noted that the minimum of the voltage does not occur exactly at the magnetic field strength where the FMR signal is zero. The voltage difference ΔV is $\Delta V \approx 0.14\mu V$.

A second measurement of the same sample in a different position in the cavity is shown in Figure 22. In this figure, the voltage curve is more asymmetric. The voltage difference is $\Delta V = 0.05\mu V$.

Figure 23 shows the dependence of the voltage V on the angle between plane of the sample and magnetic field direction. The signal is largest when the plane is parallel to the magnetic field, just as in the case of the FMR signal (see Figure 14). As predicted, the voltage changes sign when the sample is rotated by 180°. The found behaviour is in agreement with the measurements of Ando *et. al.* [17].

As can be seen in Figure 24, the voltage over the sample depends linearly on the microwave power, until saturation occurs.

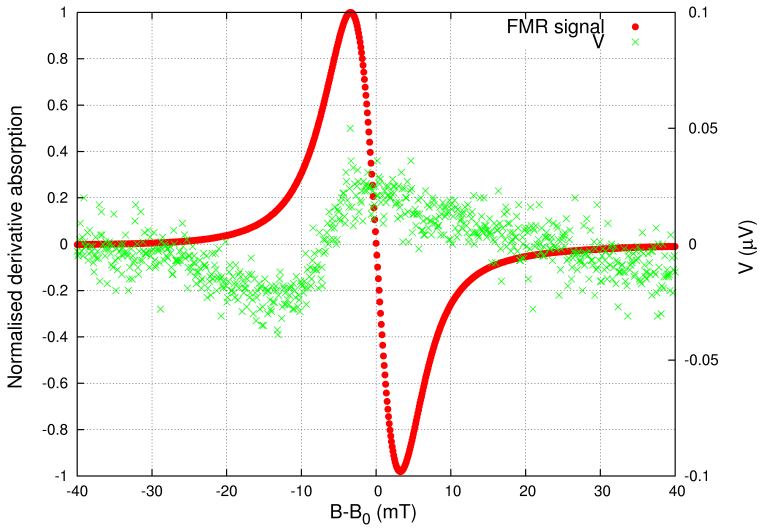

Figure 22: The voltage over the sample (crosses, right hand scale) and the normalized derivative of the absorption (closed circles, left-hand scale) as a function of the applied field B. The applied field is shifted over a value $B_0 = 64$ mT. The measurement was on the same sample as that of Figure 21, but at a different position in the cavity.

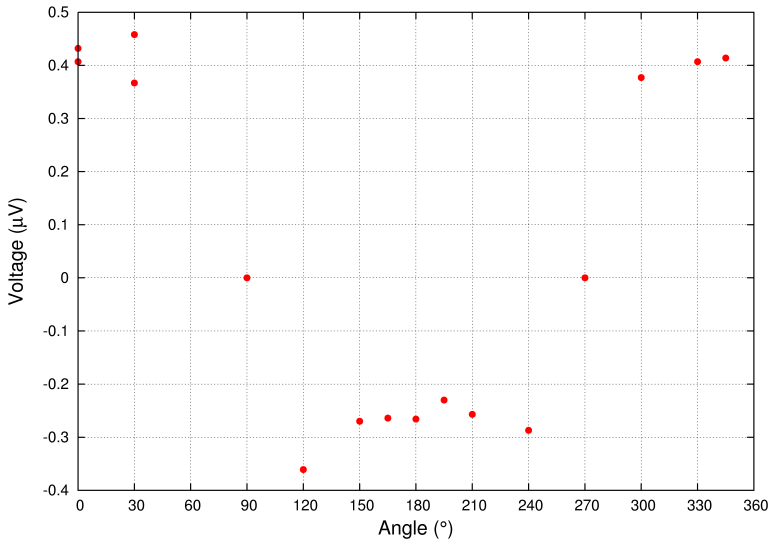

Figure 23: Voltage over the sample as a function of the angle between the magnetic field and the sample plane.

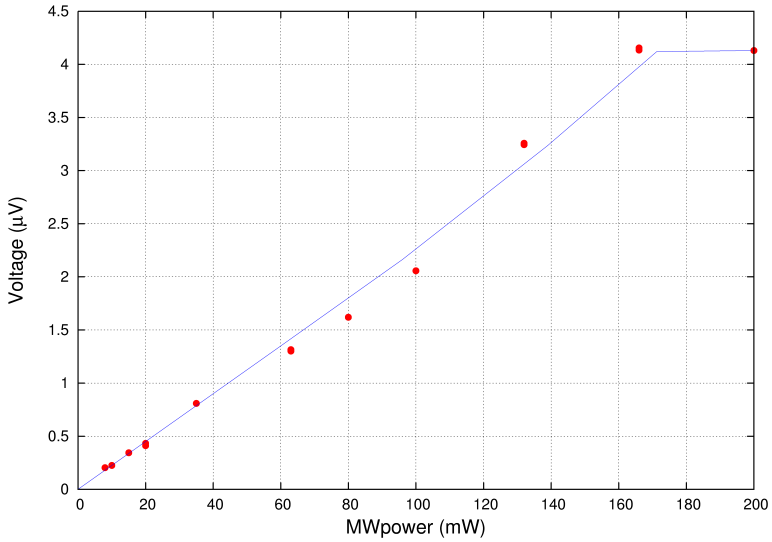

Figure 24: The dependence of voltage on the power of the microwave radiation. A line is drawn as a guide to the eye.

5 Discussion

We measured the FMR spectra of several samples consisting of Pt(10)/Co(d)/Pt(10). As can be seen in Figure 13, the spectrum is not completely symmetric. The peak is somewhat larger than the dip. This might have been caused by the shape of the sample. The boundaries of the sample affect the FMR signal. In Figure 19 the peak width as a function of the layer thickness of the Co is plotted. For d $<$ 50 nm , we have seen that the peak width falls of as a function of the sample thickness, as predicted.

However, there is a difference in the peak width of the samples consisting of Cu/Co/Pt and Pt/Co/Cu, whereas both should have one interface that absorbs spin currents from the Co layer. In the case of the Cu/Co/Pt samples, the Co layer is sputtered before the Pt layer. Between the sputtering of the two layers, approximately one minute is needed to switch targets. In this period the Co layer might oxidize, which would spoil the quality of the interface. In the case of the Pt/Co/Cu samples, the Pt layer is sputtered first. Pt oxidizes to a much smaller extent. Furthermore, the Co is presputtered in a different position right before the sputtering of the Co layer, so that it does not contain any oxidation contamination either. In this way, a better interface quality is created. This could explain the fact that the Cu/Co/Pt samples show less damping, because less spin current is flowing in these samples.
It might also explain why older samples, consistent of only bilayers (batches A-D, F and H) do not exhibit significant peak broadening. Another factor that might play a role in these samples is the difference between the growth of Co on Si and Pt, which may cause a different structure.

The peak of the voltage in Figure 21 is more or less symmetric. This indicates that the main contribution to this voltage is coming from the inverse spin Hall effect. The shifted zero with respect to the FMR signal and the partial asymmetry may be caused by the anomalous Hall effect.
The voltage difference in Figure 22 is somewhat smaller. This might be caused by the fact that the FMR signal is lower (in Figure 21 the FMR signal is clearly saturated, in this case it is not). The lower FMR intensity might be due to worse centering of the sample in the cavity. When the centering is not good, the contribution of the anomalous Hall effect is larger. This is clearly visible since the peak is much more asymmetric.
We tried to improve the centering of the sample by making an indentation in the quartz rod in which we put the sample, so that it would be exactly at the center of the cavity. However, the measurements we performed with this setup only showed more asymmetric peaks. We did not see a contribution of the inverse spin Hall effect comparable to the one in Figure 21. We therefore presume that the node of the electric field is not exactly centered at the

middle of our cavity. It would be interesting to repeat these measurements in an other cavity. Furthermore, it might be interesting to measure the voltage over the lowest Pt layer, because we think more spin current is flowing into that layer.
The voltage we measured over our sample is two orders of magnitude smaller than the voltage measured by others [18]. We think this might be because of the quality of the interfaces. Our prior FMR measurements have shown that the interface between the bottom Pt layer and the Co layer exhibits more spin pumping than the interface between the Co layer and the top Pt layer. We have measured the voltage over the top layer, so at the side where less spin current is induced. A larger voltage might be induced over the bottom Pt layer. It would also be interesting to sputter samples at ultra high vacuum in order to improve the quality of the interfaces.

6 Conclusion

We have measured the peak width of samples consistent of Pt/Co(d)/Pt. In the regime of $d \approx \min\{\lambda_{sf}, \lambda_J\}$, in our case below 10 nm the peak-to-peak width decreases almost an order of magnitude as a function of the thickness, because spin currents damp a large part of the magnetization precession in thin ferromagnetic layers. At larger thicknesses, $d > 50$ nm eddy currents cause peak broadening.
Pt/Co/Cu samples show broader peaks than Cu/Co/Pt samples, suggesting a better quality of the first interface, which allows more spin current to flow.
We have measured a voltage of 0.14μV over our sample. The peak was mainly symmetric, suggesting that it is induced by the inverse spin Hall effect. In other occurrences the peak was more asymmetric, which indicates that the anomalous Hall effect induced the voltage.
We tried to align our sample in the middle of the cavity to reduce the anomalous Hall effect, but the voltage peak became more asymmetric. Perhaps the node of the electric field is not exactly at the center of the cavity.
The voltage of 0.14μV is two orders of magnitude smaller than the voltage measured by others. This might be caused by the interface quality.

7 Acknowledgement

I am grateful to T. Verhagen and J. Aarts for supervising and helping with this project. I also thank the Fine Mechanics Department and the Electronics department for their technical support, D. Boltje and M. Hesselberth for their help with sputtering and x-ray measurements. G. van Albada, M. Huber, M. van Son and P. Gast for their help with FMR measurements and M. van Deen, J. Woudenberg and R. Leijssen for their advice in programming issues.

References

[1] M. Baibich, J. Broto, A. Fert, F. Nguyen Van Dau and F. Petroff,"Giant Magnetoresistance of (001)Fe/(001)Cr Magnetic Superlattices", Phys. Rev. Lett. bf 61, 2472 (1988)

[2] G. Binasch, P. Grünberg, F. Saurenbach and W. Zinn,"Enhanced magnetoresistance in layered magnetic structures with antiferromagnetic interlayer exchange", Phys. Rev. B bf 39, 4828 (1989)

[3] R. Adur, "Spin Pumpin in Ferromagnetic Resonance and Electrical Detection Experiments", `http://www.physics.ohio-state.edu/~adur/SpinPumping_adur.pdf` (2009)

[4] M.D. Stiles and A. Zangwill, "Anatomy of spin-transfer torque", Phys. Rev. B **66**, 014407 (2002)

[5] M. Tsoi, A. Jansen, J. Bass, W. Chiang, M. Seck, V. Tsoi and P. Wyder, "Excitation of a Magnetic Multilayer by an Electric Current", Phys. Rev. Lett. bf 80, 4281 (1998)

[6] Y. Tserkovnyak, A. Brataas, G. Bauer and B. Halperin, "Nonlocal magnetization dynamics in ferromagnetic heterostructures", Rev. Mod. Phys. **77**, 1375 (2005)

[7] K. Ando, T. Yoshino and E. Saitoh, "Optimum condition for spin-current generation from magnetization precession in thin film systems", Appl. Phys. Lett. **94**, 152509 (2002)

[8] C. Kittel,"Introduction to Solid State Physics" 8th edition, chapter 11 and 12 (2005)

[9] Y. Tserkovnyak and A. Brataas, "Enhanced Gilbert Damping in Thin Ferromagnetic Films", Phys. Rev. Lett. **88** 117601 (2002)

[10] R. Urban, B. Heinrich and G. Woltersdorf, "Semiclassical theory of spin transport in magnetic multilayers", J. Appl. Phys. **93**, 8280 (2003)

[11] O. Mosendz, "Magnetization dynamics in ultrathin magnetic films", Ph.D. Thesis, Simon Fraser University, Canada (2008)

[12] T. Taniguchi and H. Imamura, "Enhancement of the Gilbert Damping constant due to spin pumping in noncollinear ferromagnet/nonmagnet/ferromagnet trilayer systems", Phys. Rev. B **67**, 092402 (2007)

[13] S. Zhang, P.M. Levy and A. Fert, "Mechanisms of Spin-Polarized Current-Driven Magnetization Switching", Phys. Rev. Lett. **88**, 236601 (2002)

[14] K. Harii, K. Ando, H.Y. Inoue, K. Sasage and E. Saitoh, "Inverse spin-Hall effect and spin pumping in metallic films", J. Appl. Phys. **103**, 07F311 (2008)

[15] N. Mecking, "A comprehensive study of the AMR-induced microwave photovoltage, photocurrent and photoresistance in Permalloy microstrips", Ph.D. Thesis, Universität Hamburg, Hamburg (2008)

[16] T. Taniguchi, S. Yakata, H. Imamura and Y. Ando, "Penetration Depth of Spin Current in Ferromagnetic Metals", IEEE transactions on magnetics, **44**, 2636 (2008)

[17] K. Ando, Y. Kajiwara, S. Takahashi, S. Maekawa, K. Takemoto, M. Takatsu and E. Saitoh, "Angular dependence of inverse spinHall effect induced by spin pumping investigated in a Ni81Fe19/Pt thin film", Phys. Rev. B **78**, 014413 (2008)

[18] F. Czeschka, L. Dreher, M. Brandt, M. Weiler, M. Althammer, I. Imort, G. Reiss, A. Thomas, W. Schoch, W. Limmer, H. Huebl, R. Gross and S. Goennenwein, "Scaling behavior of the spin pumping effect in ferromagnet/platinum bilayers", arXiv:1012.3017v1 (2010)

A Samples

Overview of the samples used in the experiments. Each batch consists of 4 - 6 samples

Batch	Name	Layer types and thicknesses(nm)	Sputtering Base Pressure* (mbar)
A	10	Co(12)/Pt(10)	$7.9{\cdot}10^{-6}$
B	70	Co(70)/Pt(10)	$7.9{\cdot}10^{-6}$
C	60	Co(60)/Pt(10)	$4.9{\cdot}10^{-6}$
D	20	Co(20)/Pt(10)	$4.9{\cdot}10^{-6}$
E	Co10	Co(12)	$6.5{\cdot}10^{-6}$
F	Co-Pt10	Co(12)/Pt(10)	$6.5{\cdot}10^{-6}$
G	Pt-Co	Pt(10)/Co(12)	
H	Co-Pt2.10	Co(12)/Pt(10)	
I	Co-MoGe	Co(12)/MoGe(23)	$5.2{\cdot}10^{-6}$
J	PtCoPt	Pt(10)/Co(12)/Pt(10)	$5.2{\cdot}10^{-6}$
K	PtCoPt2	Pt(10)/Co(4)/Pt(10)	$5.4{\cdot}10^{-6}$
L	PtCoPt3	Pt(10)/Co(8)/Pt(10)	$5.2{\cdot}10^{-6}$
M	PtCoPt4	Pt(10)/Co(24)/Pt(10)	$5.2{\cdot}10^{-6}$
N	PtCoPt5	Pt(10)/Co(6)/Pt(10)	$5.1{\cdot}10^{-6}$
O	PtCoPt6	Pt(10)/Co(32)/Pt(10)	$5.1{\cdot}10^{-6}$
P	PtCoPt7	Pt(10)/Co(2)/Pt(10)	$5.7{\cdot}10^{-6}$
Q	PtCoPt8	Pt(10)/Co(64)/Pt(10)	$5.7{\cdot}10^{-6}$
R	PtCoPt9	Pt(10)/Co(48)/Pt(10)	$7.3{\cdot}10^{-6}$
S	PtPt	Pt(10)/Pt(10)	$7.3{\cdot}10^{-6}$
T	PtCoPt10	Pt(10)/Co(80)/Pt(10)	$8.4{\cdot}10^{-6}$
U	PtCoPt11	Pt(10)/Co(96)/Pt(10)	$8.4{\cdot}10^{-6}$
V	PtCoCu	Pt(10)/Co(5)/Cu(10)	
W	CuCoPt	Cu(10)/Co(5)/Pt(10)	
X	Co	Co(64)	$1.1{\cdot}10^{-5}$
Y	CuCoCu	Cu(10)Co(5)/Cu(10)	$1.1{\cdot}10^{-5}$
Z	Co2	Co(32)	$1.0{\cdot}10^{-5}$
a	CuCoPt2	Cu(10)Co(12)/Pt(10)	$1.0{\cdot}10^{-5}$
b	Co3	Co(12)	$1.1{\cdot}10^{-5}$
c	Co4	Co(48)	$1.1{\cdot}10^{-5}$
d	Co5	Co(4)	$1.3{\cdot}10^{-5}$
e	Co6	Co(96)	$1.3{\cdot}10^{-5}$
f	CoCu	Co(12)/Cu(10)	$1.3{\cdot}10^{-5}$
g	CoCu2	Co(4)/Cu(10)	$1.3{\cdot}10^{-5}$

*Afterwards, it turned out that the valve of the Argon mass flow controller does not completely close, so the actual base pressure is lower than the mentioned value and in the order $2 \cdot 10^{-6}$ mbar.

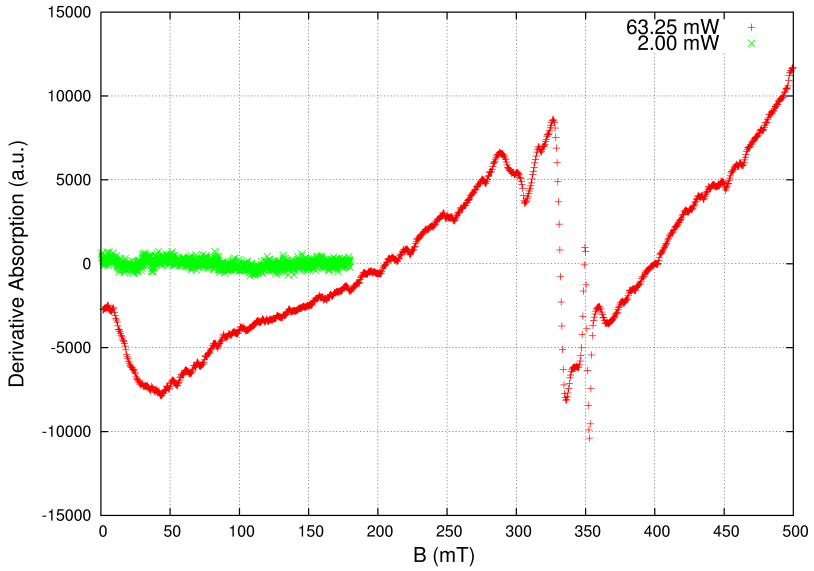

Figure 25: FMR signal of an empty cavity at high and low microwave power.

B Noise

FMR spectra of an empty cavity at low and high microwave power, a quartz tube and a quartz tube with Cu wires are shown. The FMR spectrum of the empty cavity at high microwave power indicates that some Cu powder is present in the cavity (causing the peak at 340mT) (prior to our measurements, measurements with Cu powder were often performed in the spectrometer). This does not interfere with our experiments, since we are interested in the region up to 100 mT.

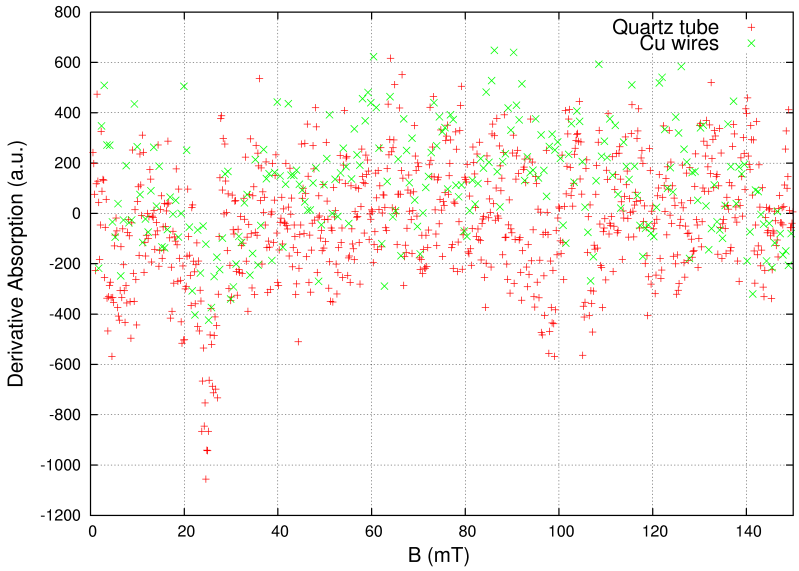

Figure 26: FMR signal of a cavity containing a quartz tube and Cu wires.